NJC

PAPER

View Article Online
View Journal | View Issue

Cite this: *New J. Chem.*, 2019, **43**, 1431

Antiparasitic activity and ultrastructural alterations provoked by organoruthenium complexes against *Leishmania amazonensis*†

Legna Colina-Vegas,[a] Joseane Lima Prado Godinho,[bc] Thallita Coutinho,[bc] Rodrigo S. Correa,[d] Wanderley de Souza,[bc] Juliany Cola Fernandes Rodrigues,[bce] Alzir Azevedo Batista*[a] and Maribel Navarro*[fg]

Received 12th September 2018,
Accepted 9th December 2018

DOI: 10.1039/c8nj04657c

rsc.li/njc

Four new organoruthenium complexes with formula $[RuCl(\eta^6\text{-}p\text{-cymene})(\mu\text{-FCZ})]_2[Cl]_2$ (**1**), $[RuCl(FCZ)(\eta^6\text{-}p\text{-cymene})(PPh_3)]PF_6$ (**2**), $[RuCl(CTZ)(\eta^6\text{-}p\text{-cymene})(PPh_3)]PF_6$ (**3**) and $[RuCl(KTZ)(\eta^6\text{-}p\text{-cymene})(PPh_3)]PF_6$ (**4**) (where FCZ: 2-(2,4-difluorophenyl)-1,3-di(1*H*-1,2,4-triazol-1-yl)-2-propanol, CTZ: 1-[(2-chlorophenyl)-diphenylmethyl-1*H*-imidazole] and KTZ: *cis*-1-acetyl-4-[4-[[2-(2,4-dichlorophenyl)-2-(1*H*-imidazol-1-ylmethyl)-1,3-dioxolan-4-yl]methoxy]phenyl]piperazine) were synthesized, characterized and evaluated as potential inhibitors for *Leishmania amazonensis* growth by widely reported methods. Complexes **3** and **4** displayed effective IC_{50} activities against *Leishmania amazonensis* promastigotes and intracellular amastigotes in the range of nanomolar concentration. Scanning and transmission electron microscopy analysis of *Leishmania amazonensis* promastigotes after treatment with 300 or 500 nM of complexes **3** and **4** for 48 h showed morphological alterations in the cell surface, a shortening of the flagellum, loss of mitochondrial matrix, disorganization of the kDNA and abnormal chromatin condensation. Thus, our strategy of incorporating a ruthenium atom into the structure of clinical drugs to improve their efficacy continues to demonstrate suitability for metallodrug discovery purposes.

Introduction

Leishmaniasis is one of the most critical neglected diseases manifested worldwide affecting 101 countries with incidence estimated at 700 000 to 1 million new cases and 20 000 to 30 000 deaths, annually. This disease is caused by protozoan parasites of the *Leishmania* genus that are transmitted to humans by over 90 sandflies species. The three different clinical manifestations of leishmaniasis lead to severe public health problems: (1) visceral leishmaniasis is usually fatal when untreated and affects children mostly; (2) mucocutaneous leishmaniasis is a mutilating disease that leads to partial or total destruction of mucous membranes; and, (3) cutaneous leishmaniasis, the most common form of the disease, is a disabling disease where several lesions can spread throughout the body.[1]

The available treatments for leishmaniasis are far from ideal. The classic first-line treatment for leishmaniasis relies on pentavalent antimonials with sodium stibogluconate (pentostam) and meglumine antimoniate (glucantime). The second-line of treatment is based on using amphotericin B (deoxycholate or liposomal) or pentamidine isethionate, which are toxic and expensive. Also, all of these drugs have several limitations, such as serious adverse effects, resistance cases, undesirable administration routes, long-term administration, and instability at high temperatures.

In 2002, miltefosine was registered as the first oral treatment for visceral leishmaniasis in India,[2] and nowadays, it's the first-line chemotherapeutic agent in some countries in Asia, Africa and Europe. Although miltefosine has 94% efficacy in Asia (India) and it is administrated by the oral route, it is teratogenic, hepatotoxic and nephrotoxic.[3] Thus, there is an urgent need to

[a] *Departamento de Química, Universidade Federal de São Carlos, São Carlos, SP, Brazil. E-mail: daab@ufscar.br*
[b] *Instituto de Biofísica Carlos Chagas Filho, Universidade Federal do Rio de Janeiro, Rio de Janeiro, Brazil*
[c] *Instituto Nacional de Ciência e Tecnologia de Biologia Estrutural e Bioimagem and Centro Nacional de Biologia Estrutural e Bioimagem-Cenabio, Universidade Federal do Rio de Janeiro, Rio de Janeiro, Brazil*
[d] *Departamento de Química, ICEB, Universidade Federal de Ouro Preto, Ouro Preto, MG, Brazil*
[e] *Núcleo Multidisciplinar de Pesquisa UFRJ-Xerém, Divisão Biologia, Campus UFRJ-Xerém, Duque de Caxias, Brazil*
[f] *Instituto Nacional de Metrologia, Qualidade e Tecnologia, INMETRO, Xerem, RJ, Brazil*
[g] *Departamento de Química, ICE, Universidade Federal de Juiz de Fora, Juiz de Fora, MG, Brazil. E-mail: maribel.navarro@ufjf.edu.br*

† Electronic supplementary information (ESI) available. CCDC 1830307 and 1830308. For ESI and crystallographic data in CIF or other electronic format see DOI: 10.1039/c8nj04657c

develop new therapeutic alternatives as the current treatment is unsatisfactory due to toxicity, limited efficacy and high cost. Another group of antileishmanial compounds are the sterol biosynthesis inhibitors, including terbinafine, imidazole derivatives (ketoconazole KTZ, clotrimazole CTZ, triazoles: fluconazole FCZ, itraconazole ITZ, and azasterols), however they are still in an experimental phase and there is not enough evidence for their use in clinical treatments.[4]

Over the past two decades, our research group has demonstrated that metal complexes with some imidazole derivatives and another type of ligand are active against several parasites responsible for neglected diseases; thus, according to this strategy, combining a well-known bioactive agent and a metal fragment into a single molecule results in a synergy that can translate into improved activity and/or selectivity against parasites.[5–8] More recently, various organoruthenium and manganese complexes with different azole antifungal agents were reported with significant antiparasitic activity at low micromolar concentrations against *Leishmania major*, *Tripanosoma cruzi* and *Schistosoma mansoni*.[9–11] Taking into account all of the above, in this work four new organoruthenium complexes with CTZ, KTZ and FCZ molecules, using triphenylphosphine and chlorido as auxiliary ligands, were synthesized and characterized looking for compounds with good biological properties. The complexes were evaluated against *Leishmania amazonensis* promastigotes and intracellular amastigotes to determine the IC_{50} values by MTS/PMS assay and characterize the morphological and ultrastructural alterations induced by the treatment of promastigotes with ruthenium(II) complexes.

Results and discussion

Synthesis and characterization

The azoles here selected are well-established ligands for transition metal complexes; in particular, CTZ and KTZ have been more reported when compared to the FCZ ligand, which can adopt two different monodentate coordination modes of the 1,2,4-triazole ring *via* N1 or N4.[12,13] The desired ruthenium complexes were obtained in good yields by similar procedures (Scheme 1), in which the reaction was carried out in methanol.

The binuclear compound $[RuCl(\eta^6\text{-}p\text{-cymene})(\mu\text{-FCZ})]_2Cl_2$ (**1**) was obtained by reaction of FCZ ligand with the chloro-bridged arene ruthenium complex $[RuCl_2(\eta^6\text{-}p\text{-cymene})]_2$; the reaction of FCZ with $[RuCl_2(\eta^6\text{-}p\text{-cymene})(PPh_3)]$, in boiling methanol, lead to the mononuclear compound $[RuCl(FCZ)(\eta^6\text{-}p\text{-cymene})(PPh_3)]PF_6$ (**2**). A similar procedure was followed to obtain complexes $[RuCl(CTZ)(\eta^6\text{-}p\text{-cymene})(PPh_3)]PF_6$ (**3**) and $[RuCl(KTZ)(\eta^6\text{-}p\text{-cymene})(PPh_3)]PF_6$ (**4**). The complexes under investigation are stable at room temperature, and soluble in common organic solvents chloroform, dichloromethane, acetone, and dimethylsulfoxide, and insoluble in water, hexane and diethyl ether. Half-sandwich complexes **2**, **3** and **4** with three-legged piano stool geometry with four different substituents [Mabcd] are examples of organometallic compounds with a stereogenic metal center.

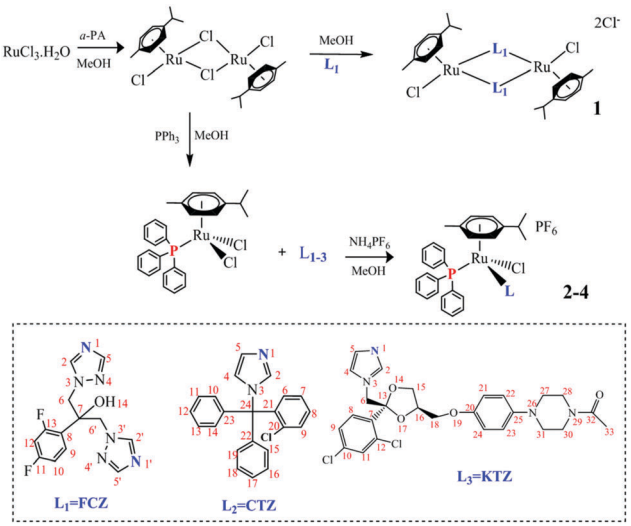

Scheme 1 Synthesis of the organometallic azole–Ru(II) complexes and ligands with numbering for NMR data. α-PA: α-phellandrene.

The UV-Vis spectra of the compounds are essentially analogous to the ruthenium starting material complexes and characterized by intense absorption bands in the UV region, at ~250 nm, characteristic of π–π* transitions of the aromatic ligands. This band was followed by one or two broad and less intense bands, which are placed between 300 and 350 nm. The solid state FT-IR spectra of the complexes presented the characteristic bands in the range of 3142–3155 ν(C–H); 1557–1586 ν(C=N); 1491–1512 ν(C=C); 840–856 ν(P–F); 557 δ(P–F); 510–527 ν(Ru–P) and 298–299 ν(Ru–Cl). The molar conductivities found, in acetone, were in the range of 2 : 1 electrolytes for complex **1** and in the range of 1 : 1 electrolytes for complexes **2–4**. Electrospray ionization mass spectra were obtained in acetone (Fig. S1, ESI†). The spectra for **1** present the fragment at a low intensity corresponding to $[M–2Cl–H]^+$ *m/z* 1153.1753 and also exhibited peaks of high intensity corresponding to the cations $[M–2Cl]^{2+}$ *m/z* 577.0665 and $[Ru(p\text{-cymene})(FCZ)]^+$ *m/z* 541.0880. The compounds provide parent peaks corresponding to the cations $[M–PF_6]^+$ *m/z* 839.1696 (**2**), 877.1675 (**3**), 1065.1963 (**4**), $[M–PPh_3–PF_6]^+$ *m/z* 615.0872 (**3**), 533.0614 (**4**) and $[M–XTZ–PF_6]^+$ *m/z* 533.0444 (**2**), 533.0698 (**3**), 497.0935 (**4**), where XTZ: FCZ, CTZ or KTZ.

All NMR signals were assigned on the basis of 1D (^{1}H and ^{13}C{1H} NMR) and 2D experiments such as Correlation Spectroscopy (^{1}H–^{1}H gCOSY), Heteronuclear Single Quantum Coherence (^{1}H–^{13}C gHSQC) and Heteronuclear Multiple Bond Coherence (^{1}H–^{13}C gHMBC). The ^{1}H NMR of binuclear complex **1** presents characteristic resonances of *p*-cymene and the fluconazole ligand as well as widening and splitting of the signals. A possible explanation for these results can be attributed to the different conformations namely *anti–gauche* (A–G) and *anti–anti* (A–A) of a fluconazole ligand (Fig. 1), which generate a fluxional molecule.[14]

The ^{1}H NMR spectra of complexes **2**, **3** and **4** show the characteristic resonances of *p*-cymene, fluconazole and triphenylphosphine ligands with a relative integral ratio of 1 : 1 : 1 and the signals typical of N-coordinated azole binds to the metal through the unsubstituted N1 atom, a good donor site of these molecules.

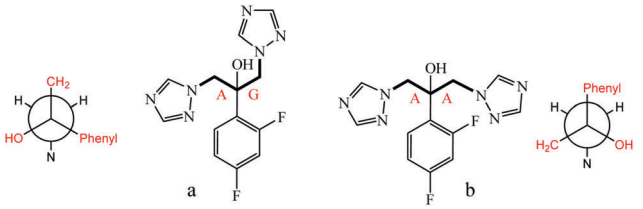

Fig. 1 Conformational isomers of fluconazole: (a) *anti–gauche*, (b) *anti–anti*.

The resonances of the *p*-cymene ring are in the characteristic range of mono-cationic Ru(II). The most remarkable characteristics of these complexes compared with the precursor $[RuCl_2(\eta^6\text{-}p\text{-cymene})(PPh_3)]$ is the chemical shift of the aromatic protons of *p*-cymene that exhibit four pairs of doublets at 6.0–5.0 ppm. This behavior was reported for other complexes such as $[Ru(\eta^6\text{-}p\text{-cymene})(O\text{-}S)Cl]$, $[Ru_2(\eta^6\text{-}p\text{-cymene})_2(EPh_3)_2(\mu\text{-}4,4'\text{-bipy})(Cl)_2]$ and $[Ru(\eta^6\text{-}p\text{-cymene})(PPh_3)(L)Cl]PF_6$ with O-S: acylthioureas, E: As or P and L: S-donor systems based on heterocyclic thiourea derivatives.[15–17] The NMR $^{31}P\{^1H\}$ spectra of the precursor $[Ru(\eta^6\text{-}p\text{-cymene})(PPh_3)Cl_2]$ present a singlet signal at 24.0 ppm corresponding to the PPh_3 ligand while the NMR $^{31}P\{^1H\}$ spectra of the complexes, after azole coordination to the ruthenium metal center, showed a significant chemical shift around 36.0 ppm and an additional heptet signal at −114.1 ppm attributed to the PF_6^- anion.

Crystal structure determination of **1** by single-crystal X-ray diffraction confirmed the formation of a binuclear complex containing two FCZ ligands making a bridge between the two-ruthenium centers. The complex crystallizes in a $P\bar{1}$ centrosymmetric space group, in which the molecule is located in a special position (inversion center). In the structure, there are two chlorides as counter-ions, per complex. The chloride anion is hydrogen bonded to the hydroxyl group of the FCZ ligand, presenting an O–H···Cl separation of 2.259 Å. This interaction displays an important role for crystal structure stabilization. Moreover, disordered methanol and water located in the cavity along the *b* axis can be observed.

As can be seen in Fig. 2, the complex presents a 20-membered macrocyclic ring with the Ru···Ru atoms at a separation of 10.103 Å. The Ru(II)–Ct distance [1.666 Å], where Ct means the centroid of

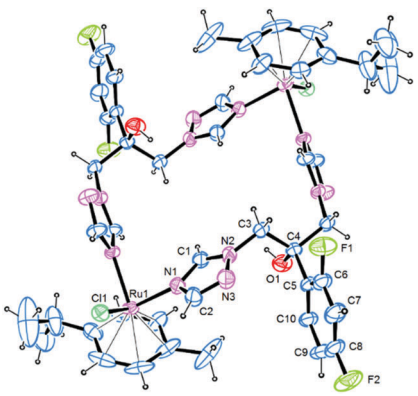

Fig. 2 Crystal structure of complex **1**, showing the ellipsoids at 30% probability. The Cl^- and disordered solvent were omitted.

Table 1 Selected bond lengths around the metal of the complexes **1** and **5**

Fragment	1	5
Ru(1)–N(1)	2.114(4)	—
Ru(1)–N(11)	2.139(3)	—
Ru(1)–Cl(1)	2.4056(10)	2.411(2)
Ru(1)–Ct	1.668(1)	1.734(3)
Ru(1)–O(1W)	—	2.144(10)
Ru(1)–P(1)	—	2.373(3)

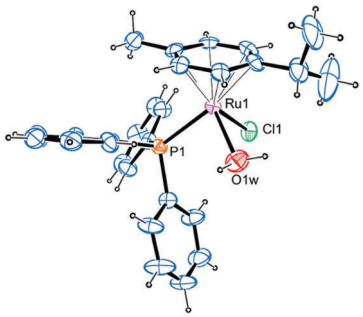

Fig. 3 Crystal structure of the complex $[RuCl(H_2O)(\eta^6\text{-}p\text{-cymene})(PPh_3)]PF_6$ (**5**), showing the ellipsoids at 30% probability. The PF_6^- was omitted.

the *p*-cymene ring, is in agreement with Ru(II)–*p*-cymene with diamine ligands.[18]

It is interesting to observe that the precursor $[RuCl_2(\eta^6\text{-}p\text{-cymene})(PPh_3)]$ used to obtain the complexes **2**, **3** and **4** showed aquation in a methanol/water solution mixture, resulting in the substitution of one chlorido by a water molecule, forming the complex $[RuCl(H_2O)(\eta^6\text{-}p\text{-cymene})(PPh_3)]PF_6$ (**5**) that also presents a stereogenic ruthenium center. In the structure of **5**, the Ru(II)–Ct distance [1.735 Å] is slightly longer compared with complex **1**, probably due to the influence of the PPh_3 ligand (Table 1). Based on the analysis of the crystal structure of the complex **5**, the presence of two molecules was established in the asymmetric unit. Both molecules are very similar. For the sake of clarity, Fig. 3, presenting an Ortep-3 type, shows the structure of just one molecule. The separation between these ligands and Ru(II) is represented in Table S2 (ESI†). Analyzing the supramolecular behavior in complex **5**, it can be observed that while the coordinated water molecule is involved in O1–Hw···F–P intermolecular interactions, the Cl– ligand does not display any interaction with it.

Antiproliferative effects on *Leishmania amazonensis* promastigotes and intracellular amastigotes

The ruthenium complexes synthesized here were tested against *Leishmania amazonensis* promastigotes and intracellular amastigotes. First of all, they were analyzed against promastigotes using two different methods: (1) MTS/PMS assay for measuring cell proliferation and viability using a sensitive quantification method based on the activity of NAD(P)H-dependent dehydrogenase enzymes in metabolically active cells; (2) cell count every 24 h in a phase contrast light microscope using the Neubauer chamber during 96 h of growth.

Table 2 IC_{50} values from MTS/PMS assay after treatment of *Leishmania amazonensis* promastigotes

Compound	IC_{50} (μM) 24 h	IC_{50} (μM) 48 h
1	≥10	≥10
2	≥10	≥10
3	0.24 ± 1.65	0.57 ± 5.30
4	0.08 ± 2.62	0.15 ± 3.35
Clotrimazole	0.82 ± 1.12	0.87 ± 1.17
Ketoconazole	≥3.00	≥3.00
Fluconazole	≥100	≥100

The MTS/PMS assay revealed significantly lower IC_{50} values (Table 2) when compared with the compounds without ruthenium. The fluconazole ligand free did not present significant activity against promastigotes, resulting in an IC_{50} higher than 100, and also complexes **1** and **2** displayed IC_{50} values higher than 10 μM. On the other hand, complex **4** was the most effective complex with an IC_{50} value of 80 nM and 150 nM for 24 h and 48 h of treatment, respectively. Complex **3** was also active against promastigotes, however it was less potent than **4**. It is interesting to compare the CTZ and KTZ ligand free complexes; the IC_{50} values were 0.87 μM and 3.00 μM after 48 h of treatment, respectively. Thus, the combination of ruthenium with azoles in *L. amazonensis* promastigotes significantly increased the activity of the compounds. To confirm the effect induced by the treatment with **3** or **4** obtained by MTS/PMS assay, we carried out experiments of growth curves counting the cells in the Neubauer chamber to follow the parasites over several days. Growth curves revealed a concentration- and time-dependent effect of **3** and **4** against promastigotes (Fig. 4), where the concentrations of 500 and 800 nM were very potent inducing around 100% growth inhibition.

Complexes **3** and **4** were also tested against *L. amazonensis* intracellular amastigotes cultivated in murine macrophages. The IC_{50} values in Table 3 were significantly lower than those found in promastigotes. For both complexes, they were in the nanomolar range. After 48 h of treatment with different concentrations, the IC_{50} values obtained were 25.8 nM and 15.5 nM for complexes **3** and **4**, respectively.

Cell viability of the macrophages was also investigated to evaluate possible cytotoxicity effects of the treatment in the mammalian host cells. The results obtained indicated that the cells began to suffer in concentrations higher than 1 μM of **4**, which was not observed for the treatment with **3** (Fig. 5A and B). Finally, we also followed the treatment of infected-macrophages with intracellular amastigotes over 48 h using a range of concentrations to describe the effect of the ruthenium complexes better and the results demonstrated that they act in a concentration-dependent manner, with activity starting at a low concentration of 10 nM (Fig. 5C and D).

Ultrastructural effects of ruthenium(II)–azole complexes on *Leishmania amazonensis* promastigotes

Electron microscopy was used to determine the morphological and ultrastructural alterations induced by ruthenium(II) complexes on promastigotes. For the analysis of the morphology of the cell body and cell surface, scanning electron microscopy was used.

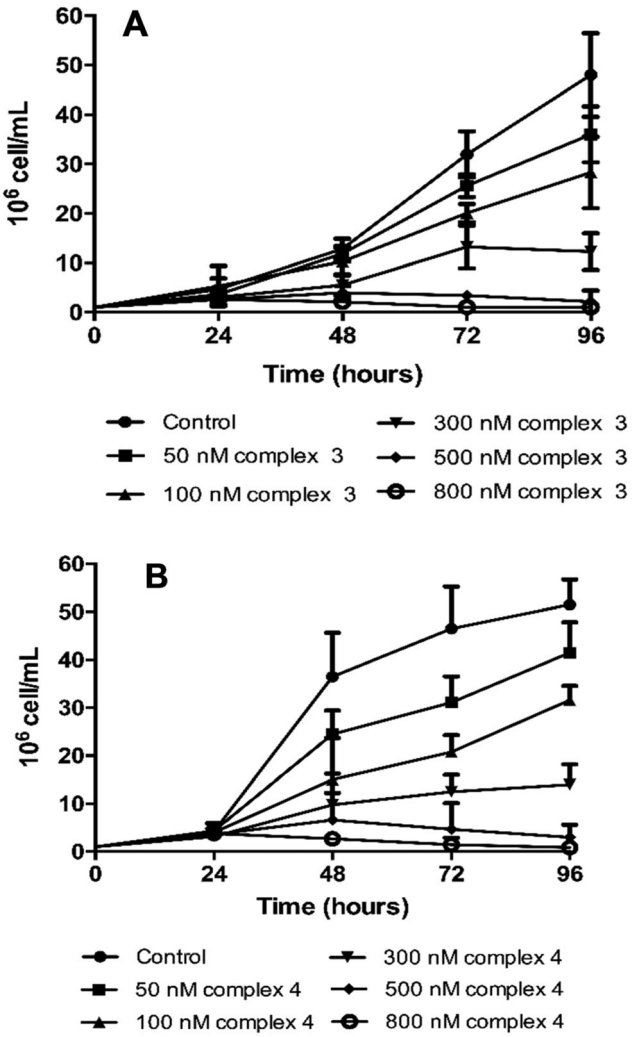

Fig. 4 Growth curves of *Leishmania amazonensis* promastigotes treated with different concentrations of (A) **3** and (B) **4** over 96 h.

Table 3 IC_{50} values obtained after treatment of *Leishmania amazonensis* intracellular amastigotes with compounds **3** and **4** for 48 h

Compound	IC_{50} (nM)	IC_{90} (nM)
3	25.80 ± 1.09	52.65 ± 1.25
4	15.53 ± 1.30	108.60 ± 2.60

Fig. 6A–F shows different images of untreated promastigotes (Fig. 6A), and treated with complexes **3** and **4** (Fig. 6B–F). The effects observed appeared to be concentration-dependent as we treated the parasites with 300 and 500 nM. For both ruthenium(II) complexes, promastigotes became rounded and swollen; some of them presented protrusions in the cell surface (arrows) and in the flagellum (arrowhead). After treatment with 300 nM complex **3** (Fig. 6B) and complex **4**, we also observed a shortening of the flagellum, however cells without a flagellum also appeared (Fig. 6D and E).

The treatment with these Ru(II) complexes was also evaluated by transmission electron microscopy trying to characterize the cellular target of the inhibitors. Fig. 7A shows a control promastigote,

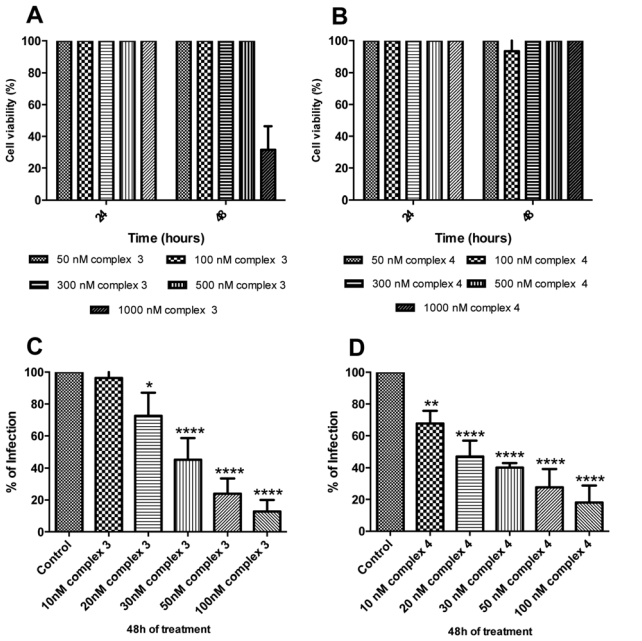

Fig. 5 Effects on cell viability of macrophages (A and B) and *L. amazonensis* intracellular amastigotes (C and D). (A and B) MTS/PMS assay was used to measure the cell viability of murine macrophages during treatment with **3** and **4** for 24 h and 48 h. Cytotoxic effects were only observed with 1 μM of **4**. (C and D) Compounds **3** and **4** were tested against *L. amazonensis* intracellular amastigotes when cultivated in murine macrophages.

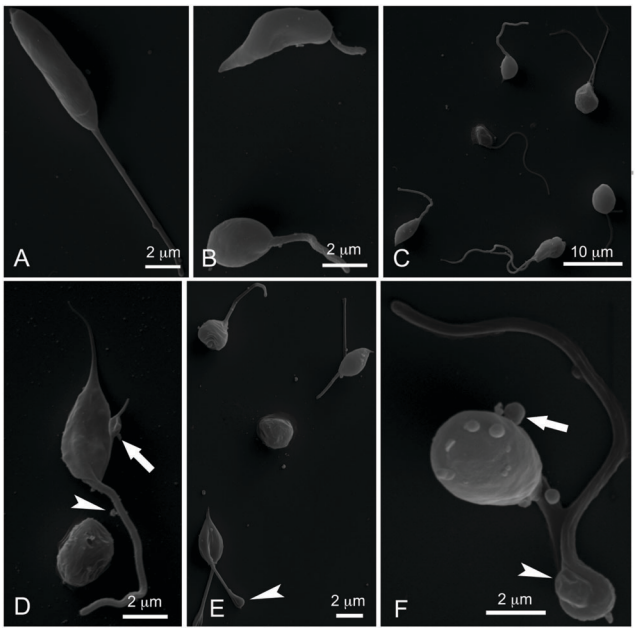

Fig. 6 Scanning electron microscopy (SEM) of *Leishmania amazonensis* promastigotes. (A) Control and (B–F) parasites treated with ruthenium complexes for 48 h. (B) 300 nM complex **3**; (C and D) 500 nM complex **3**; (E and F) 300 nM complex **4**. (A) General overview of a control parasite without any alteration in its morphology and cell surface. SEM images suggest a significant reduction in the size of the cell body, where some cells appeared rounded and swollen (B–F). We also observed the presence of membrane protrusions on the plasma membrane that covers the cell body (arrows) and the flagellum (arrowheads).

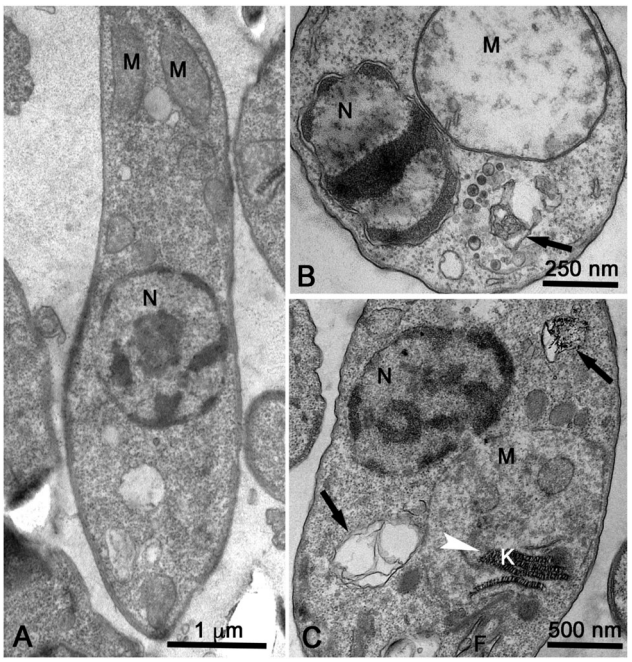

Fig. 7 Ultrathin sections of *Leishmania amazonensis* promastigotes. (A) Control and (B and C) parasites treated with complex **4** for 48 h. (A) General overview of a control parasite presenting a ramified mitochondrion (M) and nucleus (N) without any alteration in its ultrastructure. Images (B) and (C) revealed important alterations in the mitochondrion, such as: swelling and loss of the matrix content, and disorganization of the kDNA structure. We also observed abnormal chromatin condensation (B) and the presence of cytoplasmic vacuoles containing cellular debris (C, arrows). F, flagellum; N, nucleus; M, mitochondrion; K, kinetoplast.

without treatment, showing the mitochondrion and nucleus displaying a typical ultrastructure. Three kinds of alterations predominate for both complexes **4** and **3**: (1) mitochondrial swelling followed by a loss of mitochondrial matrix (Fig. 7B, C and 8A–D); (2) disorganization of the kDNA structure (Fig. 7C and 8A, B), which could be related to arrest of the cell cycle, as some cells appear to have more than one kinetoplast (arrowheads); (3) abnormal chromatin condensation (Fig. 7B and 8D), which could be related to apoptosis-like cell death. Moreover, in some cells we also observed the presence of cytoplasmic vacuoles containing membrane profiles, small vesicles and parts of the cytoplasm (Fig. 7B and C, arrows).

For other ergosterol biosynthesis inhibitors, including the group of azoles, the mitochondrion was one of the organelles most affected by the treatments.[19–22] In the Trypanosomatidae family, mitochondria have a special lipid composition, where ergosterol, episterol and 5-dehydroepisterol are essential sterols to maintain the mitochondrial membranes as shown for *Trypanosoma cruzi* epimastigotes.[23]

This special requirement could explain why mitochondria are dramatically affected after treatment with this class of compounds. An interesting alteration observed here was the effect on kDNA structure; in some of the images the kinetoplast appeared as a structure that did not divide correctly, once more than one kDNA network was observed. This should be related to a possible effect of the ruthenium(II) complexes in the DNA

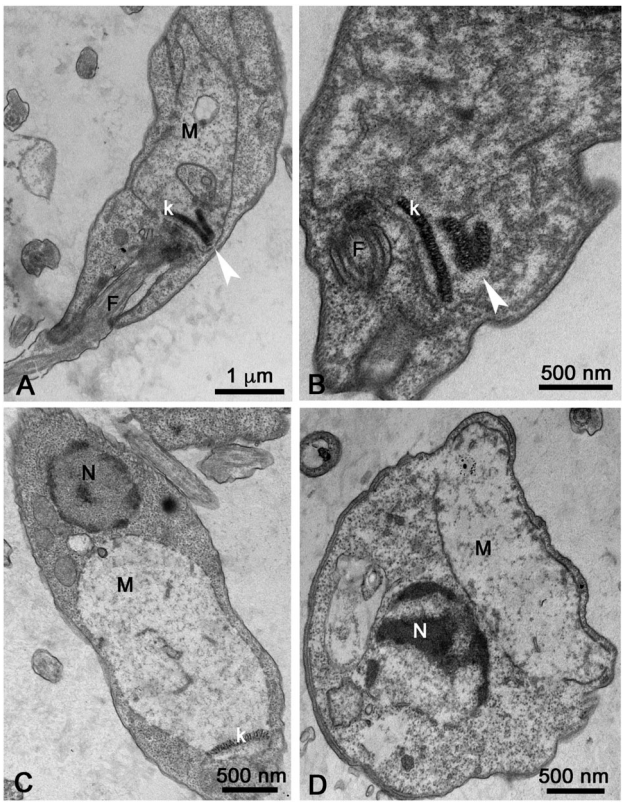

Fig. 8 Ultrathin sections of *Leishmania amazonensis* promastigotes treated with complex **3** for 48 h. (A and B) 300 nM complex **3**; (C and D) 500 nM complex **3**. As observed in complex **4**, parasites treated with complex **3** also presented significant alterations in the mitochondrion and kDNA structure. Cells appeared to present more than one kinetoplast, which may be due to cell cycle arrest. It is important to note that the nucleus also presented alterations in the chromatin condensation, as observed in D. F, flagellum; K, kinetoplast; M, mitochondrion; N, nucleus.

structure. It is important to mention that some images also suggested alterations in the chromatin condensation that could be a typical feature found in dead cells.

Thus, our results with *L. amazonensis* indicate that the coordination between azoles and the ruthenium increases the efficacy of the activity of the compound, producing a new hybrid molecule, which is much more potent against the parasite inhibiting the proliferation and inducing significant ultrastructural alterations in a nanomolar range of concentrations.

These interesting results demonstrate once more that our strategy using a synergistic effect concept can significantly increase the activity of the free ergosterol biosynthesis inhibitors (CTZ and KTZ) activity against trypanosomatid parasites when coordinated to transition metals to provide new metal–drug complexes.[12,13,24–27] This approach is an alternative way to search for new candidates to treat neglected diseases such as leishmaniasis.

Conclusions

Four ruthenium(II)–azole complexes were prepared and their characterization was achieved in both the solid state and in solution, through elemental analyses, electrospray ionization mass, UV-Vis, NMR, molar conductivity, IR spectroscopy and X-ray techniques. Single-crystal X-ray diffraction confirmed the formation of a binuclear complex $[RuCl(\eta^6\text{-}p\text{-cymene})(\mu\text{-FCZ})]_2Cl_2$ containing two FCZ ligands making a bridge between the two-ruthenium centers. Half-sandwich complexes $[RuCl(L)(\eta^6\text{-}p\text{-cymene})(PPh_3)]PF_6$ (L: FCZ, CTZ, KTZ, H_2O) are examples of chiral-at-metal organometallic compounds. The complexes $[RuCl(CTZ)(\eta^6\text{-}p\text{-cymene})(PPh_3)]PF_6$ and $[RuCl(KTZ)(\eta^6\text{-}p\text{-cymene})(PPh_3)]PF_6$ are significantly active in the inhibition of the proliferation of the *Leishmania* parasite at a very low level of concentration and both complexes increased the cytotoxic effect on promastigotes when compared to the free ligand activity. Electron microscopy images of *Leishmania amazonensis* promastigotes after treatment with the complexes showed morphological alterations such as reduction in the size of the cell body, membrane protrusions, alterations in the mitochondria including swelling and loss of the matrix content, disorganization of the kDNA structure, abnormal chromatin condensation and the presence of cytoplasmic vacuoles containing cellular debris. Further studies will be conducted to establish a better structure–activity correlation. The results obtained from this study have so far demonstrated the feasibility of the strategy to coordinate an organic molecule with the desirable biological property to a transition metal to develop an effective and alternative treatment for the *Leishmania* parasite.

Experimental section

Materials and methods

All the syntheses of the complexes were performed under an argon atmosphere. Solvents were purified by standard methods. All chemicals used were of reagent grade or comparable purity. The $RuCl_3{\cdot}3H_2O$ and α-phellandrene were purchased from Sigma-Aldrich. The ligands CTZ, KTZ and FCZ were supplied by the Calendula Pharmacy (São Paulo, Brazil). Starting materials $[RuCl_2(\eta^6\text{-}p\text{-cymene})]_2$ and $[RuCl_2(\eta^6\text{-}p\text{-cymene})(PPh_3)]$ were prepared following the method described in the literature.[28,29] The microanalyses were performed using a FISIONS CHNS, mod. EA 1108 microanalyzer. The IR spectra were recorded on an FT-IR Bomem-Michelson 102 spectrometer in the range of 4000–250 cm^{-1} using KBr pellets. Conductivity data were obtained using a Meter Lab CDM2300 instrument; measurements were taken at room temperature using 1.0 mM solutions. The UV-Vis spectra were recorded on a Hewlett Packard diode array-8452A. The electrospray mass (ESI-MS) spectra were recorded on Water Synapt HDMS TOF with a hybrid quadrupole analyzer, using acetone as a solvent. All the 1D and 2D NMR experiments (^1H, $^{13}C\{^1H\}$, $3^1P\{^1H\}$, ^1H–^1H gCOSY, ^1H–^{13}C gHSQC, ^1H–^{13}C gHMBC) were recorded at 298 K on a 9.4 T Bruker Avance III spectrometer with a 5 mm internal diameter indirect probe with ATMATM (Automatic Tuning Matching).

Synthesis of the metal complexes

$[RuCl(\eta^6\text{-}p\text{-cymene})(\mu\text{-FCZ})]_2Cl_2$ (1). A solution of $[RuCl_2(\eta^6\text{-}p\text{-cymene})]_2$ (0.20 mmol) with an excess of FCZ (0.45 mmol) was

stirred for 30 min in methanol (20 mL). The precipitated solid was filtered off and washed with methanol and diethyl ether and dried under vacuum. Yield 73%; elemental analysis (%) for $C_{46}H_{52}Cl_4F_4N_{12}O_2Ru_2{\cdot}3CH_3OH$: exp. (calc.) C 44.54 (44.55); H 5.20 (4.88); N 12.51 (12.72). IR (KBr, cm^{-1}): ν(O–H) 3421, ν(C–H) 3118, ν(C=N) 1535; ν(C=C) 1501; ν(Ru–Cl) 290. ^{1}H NMR (400 MHz, DMSO-d_6): δ (integral, attribution) 8.40 and 7.80 (4H, $H_{2,2',5,5'}$-FCZ), 7.35–6.48 (3H, $H_{9,10,12}$-FCZ), 6.10–5.40 (4H, Ph-*p*-cy), 4,60 (4H, $H_{6,6'}$-FCZ), 2.83 (1H, isopropyl-*p*-cy), 1.80 (3H, *p*-cy), 1.13 (6H, *p*-cy). $^{13}C\{^1H\}$ NMR (100 MHz, $CDCl_3$): δ ppm (attribution) 150.3–149.6 ($C_{5,5'}$-FCZ), 110.9–103.7 ($C_{9,10,12}$-FCZ), 85.8 and 82.13 (CH-Ph-*p*-cy), 56.2 ($C_{6,6'}$-FCZ), 30.9 (cisopropyl-*p*-cy), 22.2 : 20.4 ($(CH_3)_2$-*p*-cy), 18.0 (CH_3-*p*-cy). High resolution ESI(+)-MS (*m*/*z*; %) (acetone): $[M–2Cl–H]^+$ (1153.1753; 19.0), $[M–3Cl–Ru–(p\text{-cymene})–H]^+$ (833.1898; 9.52), $[M–2Cl]^{2+}$ (577.0665; 95.23), $[M–4Cl–Ru–(p\text{-cymene})–(FCZ)–H]^+$ (541.0808; 100).

General procedure for 2–4. A solution of $[RuCl_2(\eta^6\text{-}p\text{-cymene})(PPh_3)]$ (0.20 mmol) in methanol (30 mL) was stirred until complete dissolution was achieved, an excess of KPF_6 and the ligand (FCZ, CTZ or KTZ) dissolved in methanol (0.25 mmol) was added. The resultant mixture was stirred and refluxed for 8 h, and then the final yellow solutions were concentrated to *ca.* 2 mL and the solid was precipitated by addition of water. The solid obtained was filtrated off, washed with diethyl ether and water to remove the excess of the ligand or salts, and dried under vacuum. Before the biological evaluation, the stability of the complexes was tested using the $^{31}P\{1H\}$ NMR technique in DMSO or Tris–HCl solution containing 70% DMSO. After seven days, the spectra of these complexes were the same, when compared with those recorded using fresh solutions (Fig. S6, ESI†).

$[RuCl(FCZ)(\eta^6\text{-}p\text{-cymene})(PPh_3)]PF_6$ (2). Yield 78%; elemental analysis (%) $C_{41}H_{41}ClF_8N_6OP_2Ru{\cdot}H_2O$: exp. (calc.) C 46.47 (46.54); H 4.26 (4.35); N 10.94 (11.23). IR (KBr, cm^{-1}): ν(O–H) 3432, ν(C–H) 3145, ν(C=N) 1599; ν(C=C) 1502; ν(P–F) 847; δ(P–F) 558; ν(Ru–P) 512–527; ν(Ru–Cl) 305. ^{1}H NMR (400 MHz, $CDCl_3$) δ (multiplicity, integral, attribution) 8.82–7.78 (m, 4H, $H_{2,2',5,5'}$-FCZ), 7.40 (m, 15H, Ph from PPh_3), 6.80–6.62 (m, 3H, $H_{9,10,12}$-FCZ), 5.93–5.16 (m, 4H, Ph-*p*-cy), 4.82–4.30 (m, 4H, $H_{6,6'}$-FCZ), 2.40 (m, 1H, isopropyl-*p*-cy), 1,85 (m, 1H, OH-FCZ), 1.70 (m, 3H, *p*-cy), 1.19 (m, 6H, *p*-cy). $^{31}P\{^1H\}$ NMR (162 MHz, CDCl3): δ 36.65 : 36.21 (s, PPh_3), −144.15 (h, PF_6). $^{13}C\{^1H\}$ NMR (100 MHz, $CDCl_3$): δ ppm (attribution) 151.8–144.7 ($C_{2,2',5,5'}$-FCZ), 134.2–128.9 (CH–Ph–PPh_3), 129.7, 112.3 and 104.4 ($C_{9,10,11}$-FCZ), 95.0, 89.1, 87.7 and 84.8 (CH-Ph-*p*-cy), 56.1 : 55.2 ($C_{6,6'}$-FCZ), 31.0 : 29.6 (cisopropyl-*p*-cy), 22.4 : 19.6 ($(CH_3)_2$-*p*-cy), 18.27 : 18.18 (CH_3-*p*-cy). High resolution ESI(+)-MS (*m*/*z*; %) (acetone): $[M–PF_6]^+$ (839.1696; 20.00), $[M–Cl–FCZ–PF_6]^+$ (497.0852; 60.00), $[M–FCZ–PF_6]^+$ (533.0444; 100.00).

$[RuCl(CTZ)(\eta^6\text{-}p\text{-cymene})(PPh_3)]PF_6$ (3). Yield 90%; elemental analysis (%) $C_{50}H_{48}Cl_2F_6N_2OP_2Ru{\cdot}\frac{1}{2}H_2O$: exp. (calc.) C 57.50 (57.70), H 4.66 (4.65), N 2.78 (2.69). IR (KBr, cm^{-1}): ν(C–H) 3155, ν(C=N) 1570–1586; ν(C=C) 1491; ν(P–F) 840; δ(P–F) 557; ν(Ru–P) 511–526; ν(Ru–Cl) 299. ^{1}H NMR (400 MHz,$CDCl_3$) δ 7.88 (s, 1H, H_2-CTZ), 7.56–7.27 (m, 25H, Ph from CTZ and PPh_3), 6.89 (dd, J = 22.5, 7.5 Hz, 4H, $H_{6,7,8,9}$-CTZ), 6.68 (d, J = 7.9 Hz, 1H, H_5-CTZ), 6.51 (s, 1H, H_4-CTZ), 5.89 (d, J = 5.7 Hz, 1H, Ph-*p*-cy), 5.77 (d, J = 6.0 Hz, 1H from Ph-*p*-cy), 5.30 (d, J = 5.9 Hz, 1H, Ph-*p*-cy), 5.07 (d, J = 6.1 Hz, 1H, Ph-*p*-cy), 2.30–2.16 (m, 1H, isopropyl-*p*-cy), 1.14 (d, J = 6.9 Hz, 3H, *p*-cy), 1.02 (d, J = 6.8 Hz, 3H, *p*-cy). $^{31}P\{^1H\}$ NMR (162 MHz, $CDCl_3$): δ 36.24 (s, PPh_3), −144.15 (h, PF_6). $^{13}C\{^1H\}$ NMR (100.62 MHz, $CDCl_3$): δ ppm (attribution) 141.64 (C_2-CTZ), 139.29–124.01 (Cq and CH-Ph CTZ and PPh_3), 113.65 (Cq-*p*-cy), 103.55 (Cq-*p*-cy), 94.19, 90.07, 88.15 and 84.14 (CH-Ph-*p*-cy), 76.90 (C_{24}-CTZ, superposition with solvent signal), 30.59 (cisopropyl-*p*-cy), 23.27 and 20.93 ($(CH_3)_2$-*p*-cy), 18.08 (CH_3-*p*-cy). High resolution ESI(+)-MS (*m*/*z*; %) (acetone): $[M–PF_6]^+$ (877.1675; 92.20), $[M–PPh_3–PF_6]^+$ (615.0872; 71.42), $[M–CTZ–PF_6]^+$ (533.0698; 38.96), $[CTZ\text{-}Imidazol]^+$ (277.0724; 100.00).

$[RuCl(KTZ)(\eta^6\text{-}p\text{-cymene})(PPh_3)]PF_6$ (4). Yield 85%; elemental analysis (%) for $C_{54}H_{57}Cl_3F_6N_4O_4P_2Ru{\cdot}2H_2O$: exp. (calc.) C 52.48 (52.37), H 5.35 (5.19), N 4.86 (4.44). IR (KBr, cm^{-1}): ν(C–H) 3142, ν(C=N) 1557–1586; ν(C=C) 1512; ν(P–F) 851; δ(P–F) 557; ν(Ru–P) 510–527; ν(Ru–Cl) 298. ^{1}H NMR (400 MHz, $CDCl_3$) δ 7.58 (s, 1H, H_2-KTZ), 7.49–7.17 (m, 19H, Ph from KTZ and PPh_3), 7.03 (d, J = 9.0 Hz, H_5-KTZ), 6.94 (d, J = 9.0 Hz, H4-KTZ), 6.87–6.76 : 6.66 (m, 3H, $H_{8,9,11}$-KTZ), 5.98, 5.91, 5.86 and 5.78 (d, J = 6.0 Hz, 2H, Ph from *p*-cy), 5.28, 5.22, 5.18 and 5.05 (d, J = 6.0 Hz, 2H, Ph from *p*-cy), 4.37–3.60 (m, 11H, $H_{6,15,16,18,27,31}$-KTZ), 3.06 (m, 4H, $H_{28,30}$-KTZ), 2.31 (m, 1H, isopropyl *p*-cy), 2.12 : 211 (s, 3H, H_{33}-KTZ), 1.61 : 1.60 (s, 3H, *p*-cy), 0.97 (m, 6H, *p*-cy). $^{31}P\{^1H\}$ NMR (162 MHz, $CDCl_3$): δ 36.70 : 36.61 (s, PPh_3), −144.15 (h, PF_6). $^{13}C\{^1H\}$ NMR (100 MHz, $CDCl_3$): δ ppm (attribution) 169.10 (C_{32}-KTZ), 153.02–115.06 (CH-Ph and Cq of KTZ, PPh_3), 107.31 : 101.01 (Cq-*p*-cy), 103.52 : 103.03 (Cq-*p*-cy), 94.80 : 94.33, 90.29 : 90.25, 87.21 : 87.03 and 83.74 : 83.37 (CH-Ph-*p*-cy), 74.96 : 74.46, 67.67, 52.24 : 51.75 ($C_{6,15,16,18,27,31}$-KTZ), 50.97-41.37 ($C_{28,30}$-KTZ), 31.12 : 30.73 (cisopropyl-*p*-cy), 21.33 (C_{33}-KTZ), 23.21 : 22.71 and 20.58 (–$(CH_3)_2$-*p*-cy), 18.19 : 18.11 (CH_3-*p*-cy). High resolution ESI(+)-MS (*m*/*z*; %) (acetone): $[M–PF_6]^+$ (1065.1963; 71.42), $[M–PPh_3–PF_6]^+$ (803.1275; 37.66), $[M–KTZ–PF_6]^+$ (533.0614; 100.00), $[M–KTZ–PF_6–Cl]^+$ (497.0935; 71.42).

$[RuCl(H_2O)(\eta^6\text{-}p\text{-cymene})(PPh_3)]PF_6$ (5). A solution of $[RuCl_2(\eta^6\text{-}p\text{-cymene})(PPh_3)]$ (0.20 mmol) in methanol/water (2 : 1) was stirred until complete dissolution was achieved, and then an excess of KPF_6 was added, and red crystals were obtained. Yield 73%; elemental analysis (%) for $RuC_{28}H_{31}ClF_6OP_2$: exp. (calc.) C 48.63 (48.32), H 4.32 (4.49). IR (KBr, cm^{-1}): ν(C–H) 3142, ν(C=C) 1523; ν(P–F) 850; δ(P–F) 556; ν(Ru–P) 527–510; ν(Ru–Cl) 295. ^{1}H NMR (400 MHz, DMSO-d_6) δ 7.56 (m, 15H, Ph form PPh_3), 5.87 (d, J = 6.0 Hz, 2H, Ph from *p*-cy), 5.59 (d, J = 6.0 Hz, 2H, Ph from *p*-cy), 5.34 (d, J = 6.4 Hz, 2H, Ph from *p*-cy), 5.10 (d, J = 6.0 Hz, 2H, Ph from *p*-cy), 2.61 (m, 1H from isopropyl *p*-cy), 1.88 (s, 3H, *p*-cy), 1.15 (t, 6H, *p*-cy). $^{31}P\{^1H\}$ NMR (162 MHz, DMSO-d_6): δ ppm (multiplicity, attribution) 33.07 (s, PPh_3), −144.50 (h, PF_6).

Single crystal X-ray structure data analysis

Data collection and processing of the X-ray diffraction studies were performed in a Nonius Kappa-CCD diffractometer, Mo Kα (λ = 0.71073 Å), graphite monochromator, T = 298 K. The COLLECT[30] and SCALEPACK[31] programs were used to refine the cells and in all cases, all the reflections were used to obtain

the final parameters of the cell. The data were reduced using the DENZO-SMN and SCALEPACK programs. A Gaussian method implemented in WinGX was used for the absorption correction.[32,33] Using Olex2,[34] the structure was solved with the SIR2004[35] structure solution program using Direct Methods and refined with the ShelXL-2018/3[36] refinement package using Least Squares minimisation. All non-hydrogen atoms were refined with anisotropic displacement parameters. The hydrogen atoms were located from the difference synthesis of electron density and refined using the riding model on their parent atoms with $U_{iso}(H) = 1.5U_{eq}$ for water and methyl H atoms or $1.2U_{eq}$ for the remaining aromatic and methine H atoms. The voids (188.4 Å^3) in the structure **1** contain disordered solvent at partial occupancy. A satisfactory disorder model for the solvent was not found, and therefore the OLEX2 Solvent Mask routine (similar to PLATON/SQUEEZE) was used to mask out the disordered density. The ORTEP-3[37] was used to generate the molecular graphics. The X-ray crystallographic data for the structures of complexes **1** and **5** reported in this article have been deposited at the Cambridge Crystallographic Data Centre (CCDC) under deposition numbers 1830307 and 1830308, respectively.†

Anti-*Leishmania* activities

Parasite. *Leishmania amazonensis* WHOM/BR/75/JOSEFA strain was used in this study. It was isolated in 1975 from a patient with diffuse cutaneous leishmaniasis by Dr Cesar A. Cuba–Cuba (Brasilia University, Brazil) and kindly provided by the *Leishmania* Collection of the Instituto Oswaldo Cruz (Code IOCL 0071 – FIOCRUZ). Parasites were maintained after inoculation of metacyclic infective promastigotes at the base of the tail of Balb/C mice. Intracellular amastigotes were isolated from the lesions and then differentiated into promastigotes, which were maintained in Warren's medium (Brain Heart Infusion plus 20 μg mL^{-1} hemin and 10 μg mL^{-1} folic acid) supplemented with 10% of fetal bovine serum (Cultlab®) at 25 °C. Infective metacyclic promastigotes were used to infect murine macrophages to obtain intracellular amastigotes.

Antiproliferative effects against *Leishmania amazonensis* promastigotes and intracellular amastigotes. For promastigote assays, two different analyses were carried out: (1) growth curve counting of the parasite cell number in a Neubauer chamber by contrast phase light microscopy; (2) MTS/PMS assay to determine the cell viability. Growth curves of *L. amazonensis* promastigotes were initiated with an inoculum of 1.0×10^6 cells per mL in a Warren culture medium supplemented with 10% fetal bovine serum. After 24 h of growth, different concentrations of the compounds were added and the cells were cultured for 96 h, with the cell density calculated every 24 h by counting the number of cells in a Neubauer chamber using contrast phase light microscopy. Cell viability of promastigotes was evaluated by CellTiter 96® Aqueous MTS Assay (Promega, United States) (1). Regarding this, promastigotes were cultured in Warren's medium starting from a cell density of 1.0×10^6 cells per mL in 24-well plates; after 24 h of growth, different concentrations of the compounds were added to the cultures. Cell viability was measured in triplicate, in a 96-well plate, after their incubation for 24 h, 48 h and 72 h. The MTS/PMS assay reaction was quantified by optical density measurement at 490 nm in a microplate reader and SpectraMax M2/M2e spectrofluorometer (Molecular Devices, United States). As a negative control, parasites were fixed with 0.4% nascent formaldehyde for 10 min at room temperature before incubation. Data were plotted and subjected to statistical analysis using Prism 4 (GraphPad software). For intracellular amastigote assays, murine macrophages and parasites were obtained as published previously.[38] After 24 h of initial infection, different concentrations of the compounds were added, and the medium with the drug was changed every day for 3 days. After each time, cultures were fixed in Bouin's solution (70% picric acid, 5% acetic acid and 25% formaldehyde in aqueous solution), washed with 70% ethanol, followed by washing in distilled water, and then stained with Giemsa solution for 1 h. The number of intracellular amastigotes and macrophages (infected or not) was counted *via* light microscopy. Association indices (the mean number of parasites internalized multiplied by the percentage of infected macrophages divided by the total number of macrophages) were determined and used as a parameter to calculate the percentage of infection for each condition used in this study. The concentration that inhibited 50% of growth (IC_{50}) was calculated. At least three independent experiments were performed for each treatment.

Electron microscopy. Control and treated promastigotes were fixed for at least 2 h in 2.5% glutaraldehyde (Sigma Chemical Co.) in a 0.1 M cacodylate buffer (pH 7.2), and post-fixed in a solution containing 1% OsO4, 1.25% potassium ferrocyanide, 5 mM $CaCl_2$, and 0.1 M cacodylate buffer (pH 7.2) for 30 min. For scanning electron microscopy (SEM), cells were dehydrated in an ethanol series (50%, 70%, 90% and 100%; last one for 3 times), critical point dried in CO_2, mounted on stubs, sputtered with a thin gold layer, and observed under a ZEISS EVO scanning electron microscope. For transmission electron microscopy (TEM), cells were dehydrated in an acetone series (50%, 70%, 90%, and 100%; last one for 3 times) and embedded in epoxy resin. Ultrathin sections were stained with uranyl acetate and lead citrate and then observed under an FEI Tecnai T20 electron microscope.

Conflicts of interest

There are no conflicts to declare.

Acknowledgements

The authors are grateful to Fundação de Amparo à Pesquisa do Estado de São Paulo (FAPESP), Fundação Carlos Chagas Filho de Amparo à Pesquisa do Estado do Rio de Janeiro (FAPERJ) and Conselho Nacional de Desenvolvimento Científico e Tecnológico (CNPq) for the financial suport. This study was financed in part by Coordenação de Aperfeiçoamento de Pessoal de Nível Superior-Brasil (CAPES)-Finance code 001. Legna Colina-Vegas thanks to FAPESP for her postdoctoral fellowship (grant #2016/23130-5 and #2017/23254-9). R. S. Correa would like to

thank CNPq for financial support (project 403588/2016-2 and 308370/2017-1).

References

1 World Health Organization, http://www.who.int/leishmaniasis/en/.
2 T. P. Dorlo, M. Balasegaram, J. H. Beijnen and P. J. de Vries, *J. Antimicrob. Chemother.*, 2012, **67**, 2576–2597.
3 J. P. B. de Menezes, C. E. S. Guedes, A. L. O. A. Petersen, D. B. M. Fraga and P. S. T. Veras, *BioMed Res. Int.*, 2015, **2015**, 815023.
4 A. Khamesipour, *Expert Opin. Biol. Ther.*, 2014, **14**, 1641–1649.
5 R. A. Sánchez-Delgado, M. Navarro, K. Lazardi, R. Atencio, M. Capparelli, F. Vargas, J. A. Urbina, A. Bouillez, A. F. Noels and D. Masi, *Inorg. Chim. Acta*, 1998, **275–276**, 528–540.
6 M. Navarro, T. Lehmann, E. J. Cisneros-Fajardo, A. Fuentes, R. A. Sánchez-Delgado, P. Silva and J. A. Urbina, *Polyhedron*, 2000, **19**, 2319–2325.
7 T. Macedo, L. Colina-Vegas, M. da Paixão, M. Navarro, B. C. Barreto, P. C. M. Oliveira, S. G. Macambira, M. Machado, M. Prudencio, S. D'alessandro, N. Basilico, D. R. M. Moreira, A. A. Batista and M. B. P. Soares, *Parasitology*, 2016, **143**, 1543–1556.
8 T. Macedo, W. Villarreal, C. Couto, D. R. M. Moreira, M. Navarro, M. Machado, M. Prudêncio, A. A. Batista and M. B. P. Soares, *Metallomics*, 2017, **9**, 1548–1561.
9 E. Iniguez, A. Sanchez, M. A. Vasquez, A. Martínez, J. Olivas, A. Sattler, R. A. Sanchez-Delgado and R. A. Maldonado, *J. Biol. Inorg. Chem.*, 2013, **18**, 779–790.
10 P. V. Simpson, C. Nagel, H. Bruhn and U. Schatzschneider, *Organometallics*, 2015, **34**, 3809–3815.
11 J. Kljun, A. J. Scott, T. L. Rižner, J. Keiser and I. Turel, *Organometallics*, 2014, **33**, 1594–1601.
12 E. Reisner, B. V. Arion, M. F. C. Guedes da Silva, R. Lichtenecker, A. Eichinger, B. K. Keppler, V. Y. Kukushkin and A. J. L. Pombeiro, *Inorg. Chem.*, 2004, **43**, 7083–7093.
13 M. Kumar, J. Pasquale, N. J. White, M. Zeller and E. T. Papish, *Organometallics*, 2013, **32**, 2135–2144.
14 Y. Ling, L. Zhang, J. Li, S. Fana and M. Dub, *Cryst. Eng. Commun.*, 2010, **12**, 604–611.
15 K. M. Rao and P. Sarkhel, *Indian J. Chem.*, 2001, **40A**, 760–762.
16 M. Hanif, M. A. H. Nawaz, M. V. Babak, J. Iqba, A. Roller, B. K. Keppler and C. G. Hartinger, *Molecules*, 2014, **19**, 8080–8092.
17 L. Colina-Vegas, L. Luna-Dulcey, A. M. Plutín, E. E. Castellano, M. R. Cominetti and A. A. Batista, *Dalton Trans.*, 2017, **46**, 12865–12875.
18 L. Colina-Vegas, W. Villarreal, M. Navarro, C. R. de Oliveira, A. E. Graminha, P. I. S. Maia, V. M. Deflon, A. G. Ferreira, M. R. Cominetti and A. A. Batista, *J. Inorg. Biochem.*, 2015, **153**, 150–161.
19 S. T. de Macedo-Silva, W. de Souza and J. C. F. Rodrigues, *Curr. Med. Chem.*, 2015, **22**, 2186–2198.
20 J. C. F. Rodrigues, C. F. Bernardes, G. Visbal, J. A. Urbina, A. E. Vercesi and W. de Souza, *Protist*, 2007, **158**, 447–456.
21 S. T. de Macedo-Silva, T. L. A. de Oliveira-Silva, J. A. Urbina, W. de Souza and J. C. F. Rodrigues, *Mol. Biol. Int.*, 2011, **2011**, 876021.
22 S. T. de Macedo-Silva, J. A. Urbina, W. de Souza and J. C. F. Rodrigues, *PLoS One*, 2013, **8**, e83247.
23 C. O. Rodrigues, R. Catisti, S. A. Uyemura, A. E. Vercesi, R. Lira, C. Rodriguez, J. Urbina and R. Docampo, *J. Eukaryotic Microbiol.*, 2001, **48**, 588–594.
24 J. A. Urbina, *Drugs Future*, 2010, **5**, 409–419.
25 M. Navarro, C. Gabbiani, L. Messori and D. Gambino, *Drug Discov. Today*, 2010, **15**, 1070–1078.
26 E. Iniguez, A. Varela-Ramirez, A. Martínez, C. L. Torres, R. A. Sánchez-Delgado and R. A. Maldonado, *Acta Trop.*, 2016, **164**, 402–410.
27 A. Martínez, T. Carreon, E. Iniguez, A. Anzellotti, A. Sánchez, M. Tyan, A. Sattler, L. Herrera, R. A. Maldonado and R. A. Sánchez-Delgado, *J. Med. Chem.*, 2012, **55**, 3867–3877.
28 M. A. Bennett, T. N. Huang, T. W. Matheson and A. K. Smith, *Inorg. Synth.*, 1982, **21**, 74–78.
29 E. Hodson and S. J. Simpson, *Polyhedron*, 2004, **23**, 2695–2707.
30 Enraf-Nonius COLLECT, Nonius BV, Delft, The Netherlands, 1997–2000.
31 Z. Otwinowski and W. Minor, *Methods Enzymol.*, 1997, **276**, 307–326.
32 L. J. Farrugia, *J. Appl. Crystallogr.*, 1999, **32**, 837–838.
33 P. Coppens, L. Leiserowitz and D. Rabinovich, *Acta Crystallogr.*, 1965, **18**, 1035–1038.
34 O. V. Dolomanov, L. J. Bourhis, R. J. Gildea, J. A. K. Howard and H. Puschmann, *J. Appl. Crystallogr.*, 2009, **42**, 339–341.
35 M. C. Burla, R. Caliandro, M. Camalli, B. Carrozzini, G. L. Cascarano, L. De Caro, C. Giacovazzo, G. Polidori, D. Siliqi and R. Spagna, *J. Appl. Crystallogr.*, 2007, **40**, 609–613.
36 G. M. Sheldrick, *Acta Crystallogr., Sect. C: Struct. Chem.*, 2015, **71**, 3–8.
37 L. J. Farrugia, *J. Appl. Crystallogr.*, 1997, **30**, 565.
38 J. L. Godinho, K. Georgikopoulou, T. Calogeropoulou, W. de Souza and J. C. A. Rodrigues, *Exp. Parasitol.*, 2013, **135**, 153–165.